

Cancer Cell, Volume 42

Supplemental information

**Cancer-associated fibroblast phenotypes
are associated with patient outcome
in non-small cell lung cancer**

Lena Cords, Stefanie Engler, Martina Haberecker, Jan Hendrik Rüschoff, Holger Moch, Natalie de Souza, and Bernd Bodenmiller

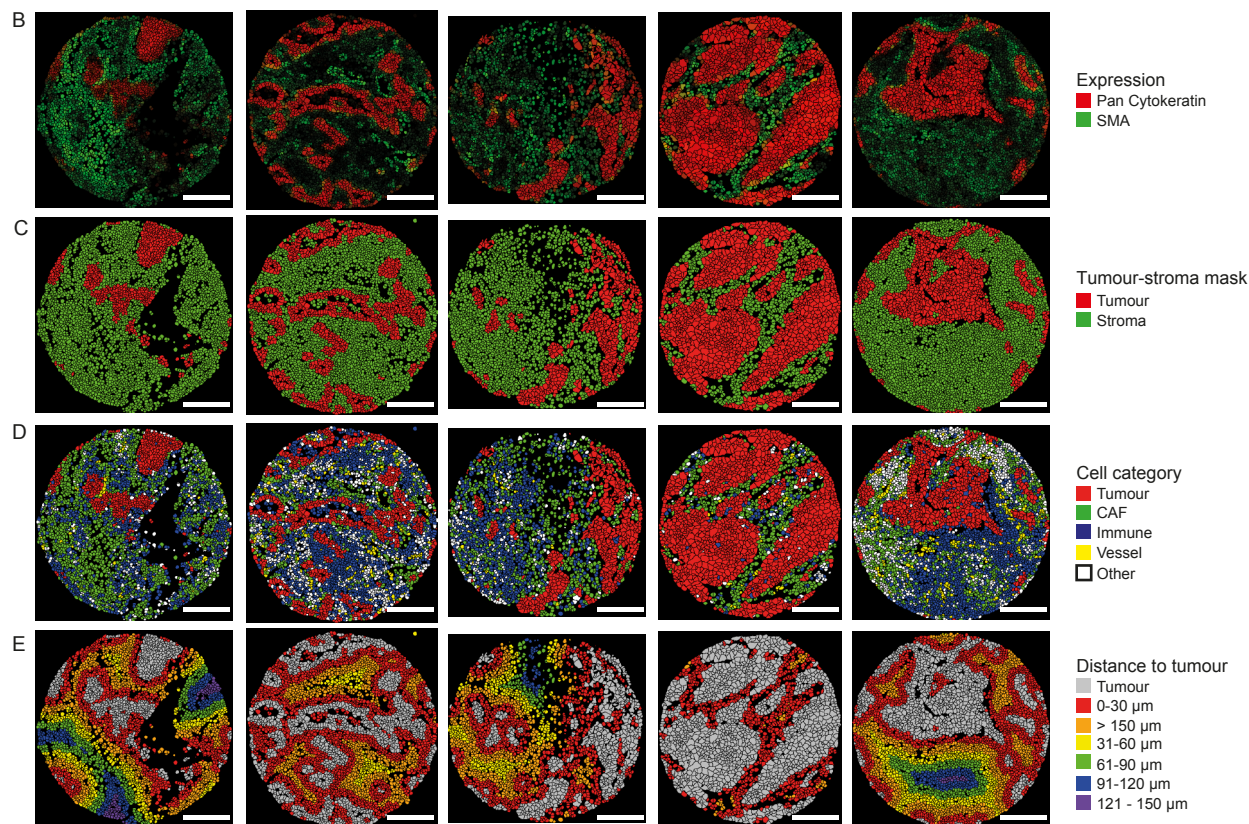
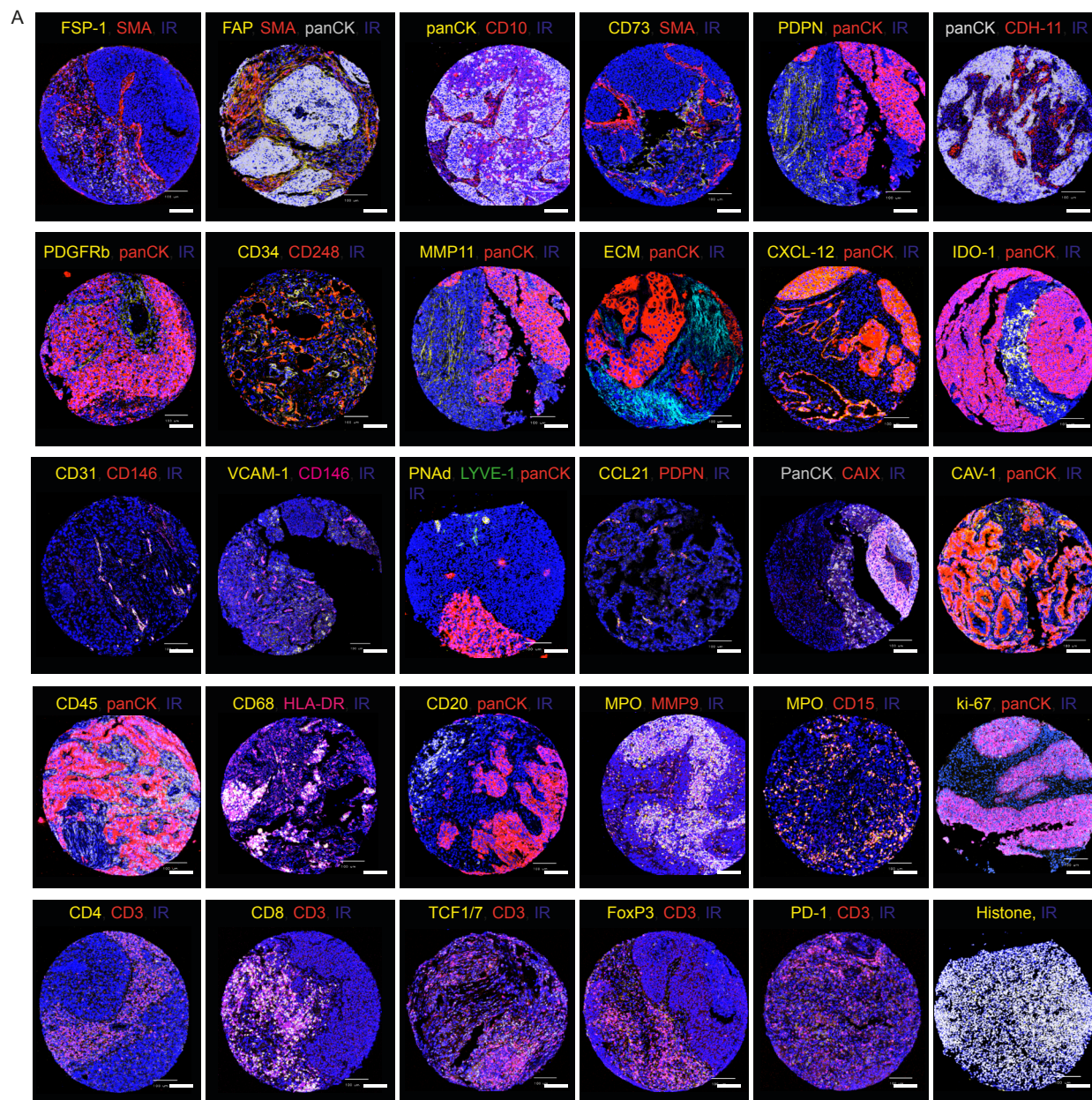


Figure S1 – Marker expression in IMC images. Related to figures 1 and 2.

- A) Representative images of all markers. Scale bars indicate 100 μm .
- B) Cell masks coloured by the mean SMA (green) and panCK (red) expression per cell. Scale bars indicate 170 μm .
- C) Cell masks pseudo-coloured stromal (green) or tumour (red) compartment. Scale bars indicate 170 μm .
- D) Cell masks pseudo-coloured by cell category: tumour (red), immune (blue), fibroblast (green), vessel (yellow), other (white). Scale bars indicate 170 μm .
- E) Cell masks pseudo-coloured by the distance from each cell to the closest tumour stroma border: tumour (white), 0-30 μm (red), 31-60 μm (orange), 61-90 μm (yellow), 91-120 μm (green), 121-150 μm (blue), > 150 μm (purple). Scale bars indicate 170 μm .

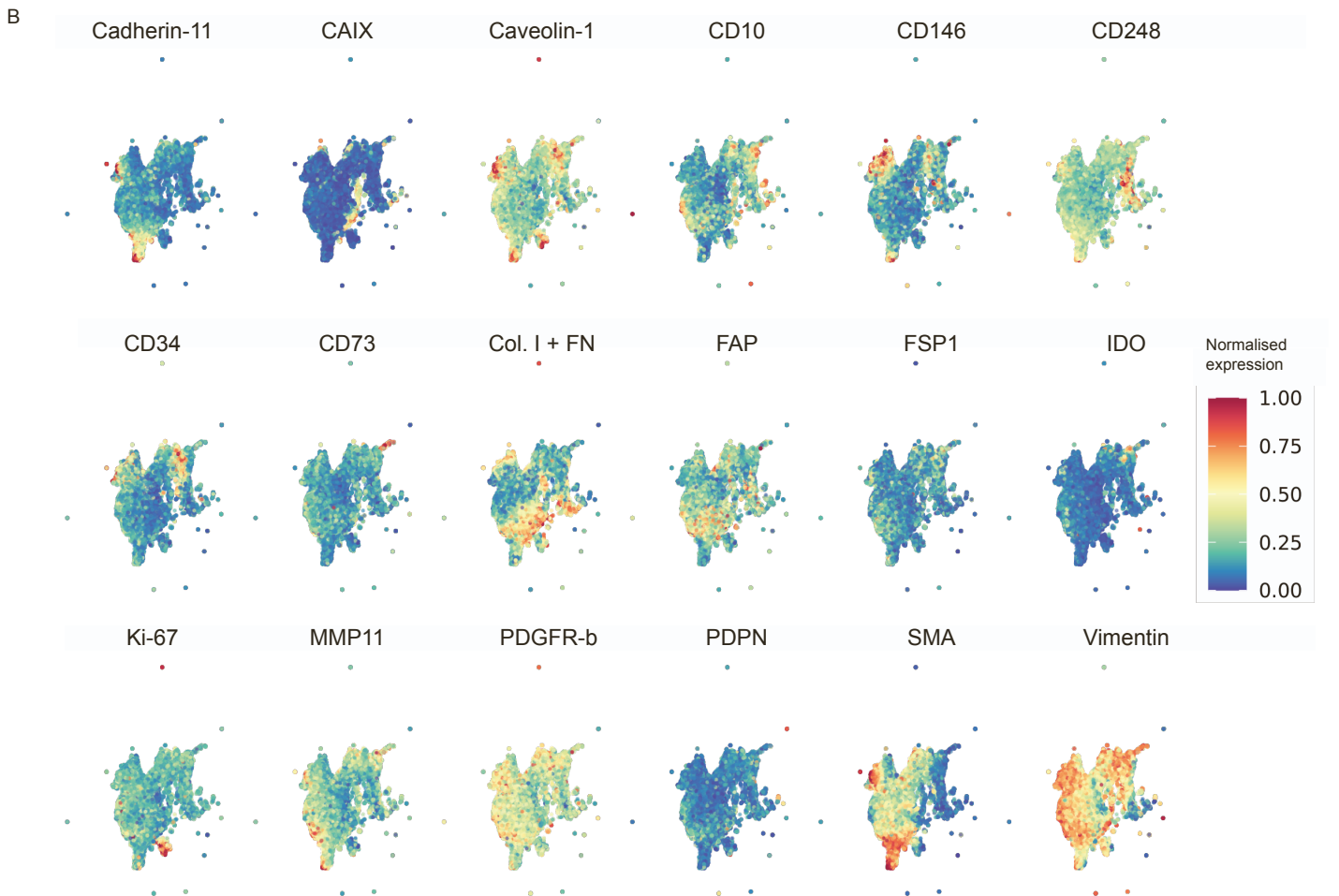
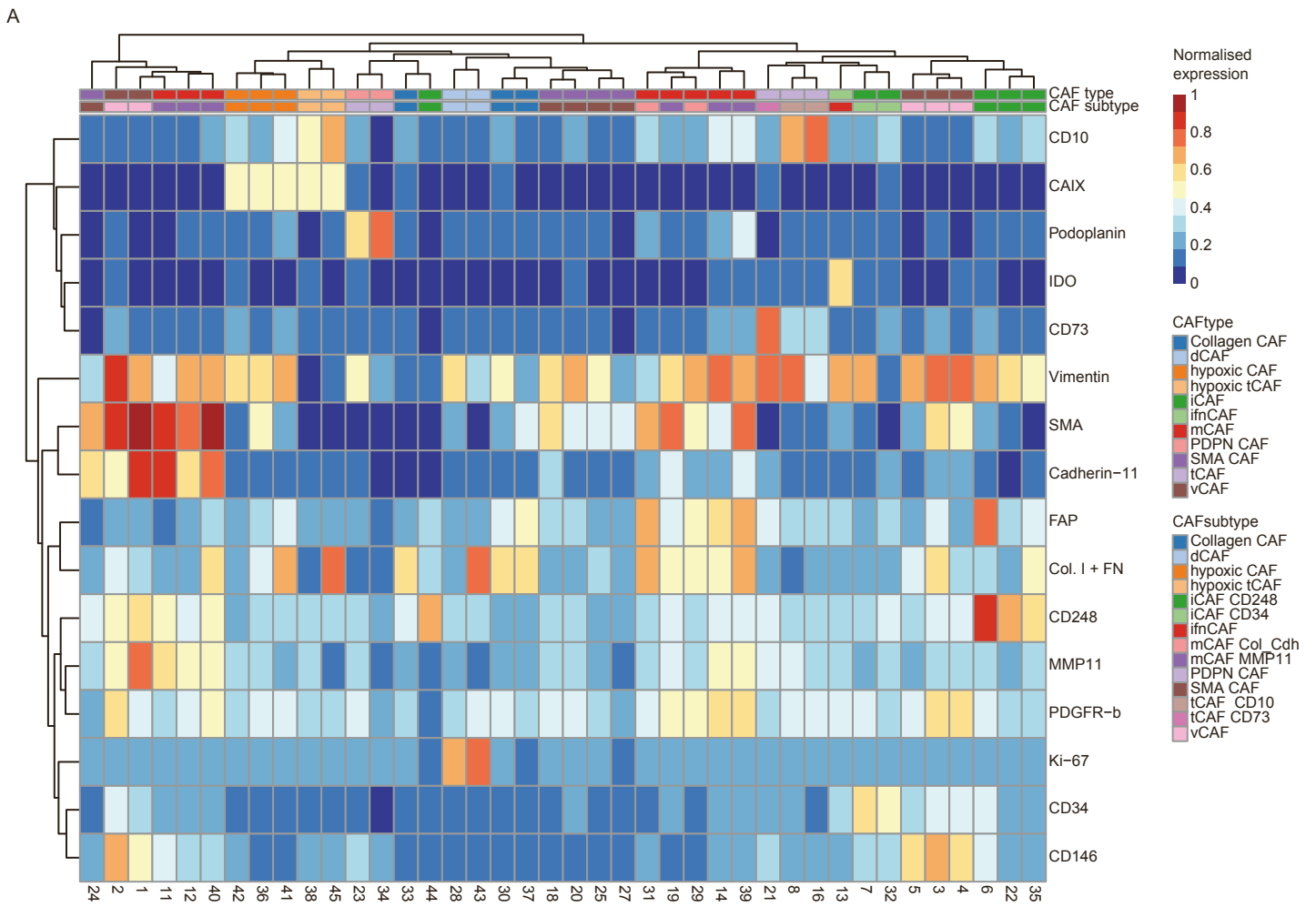


Figure S2 – CAF phenotyping. Relates to Figure 3.

- A) Heatmap of expression levels of CAFs clustered with FLOWSOM (k max = 45, som = 40) together with CAF type and CAF subtype.
- B) UMAP of a random subset of 200,000 cells of all fibroblasts showing the mean intensity per cell scaled from 0-1 for all CAF markers.

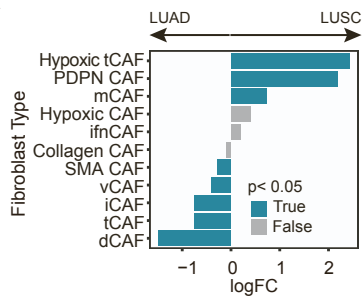
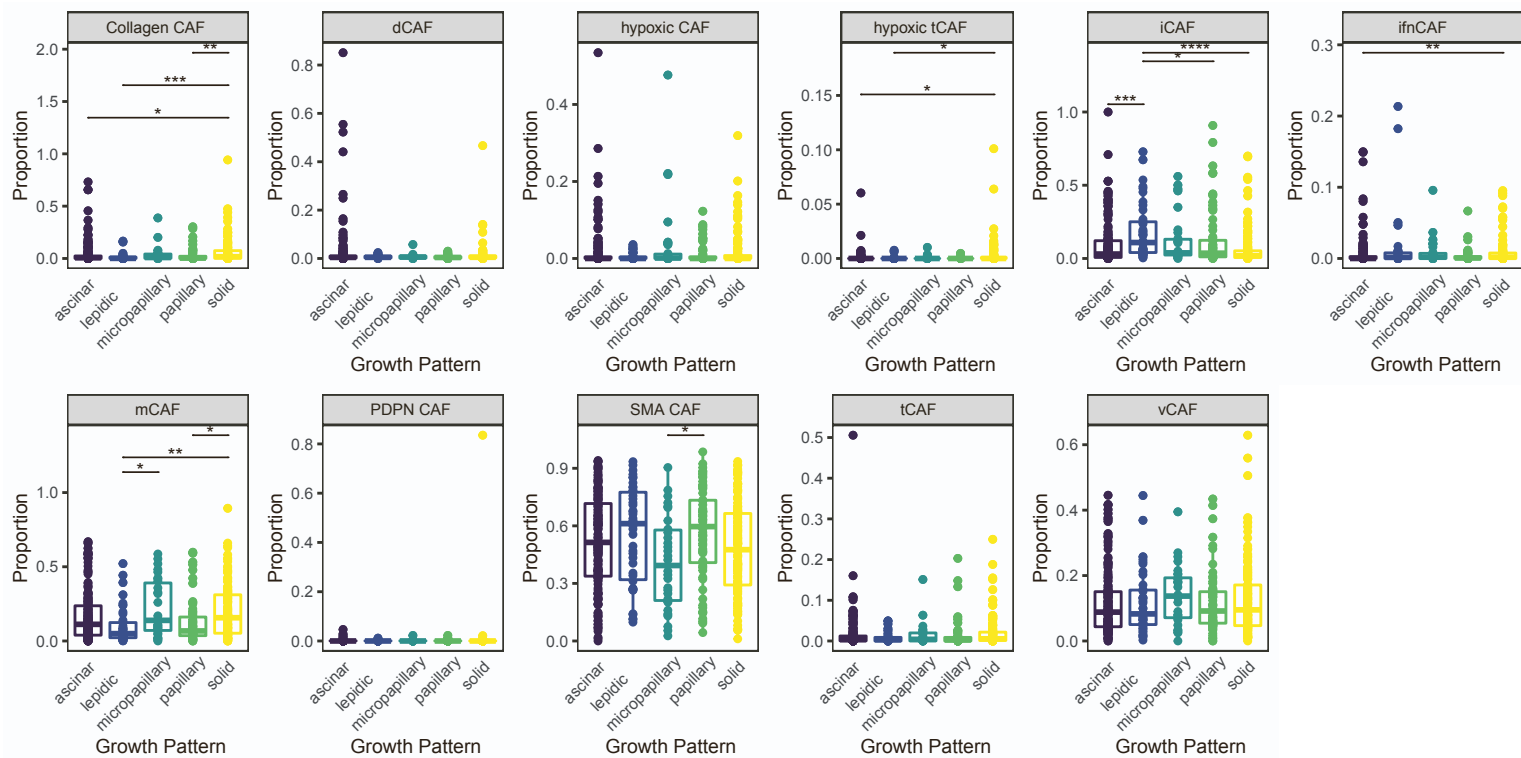
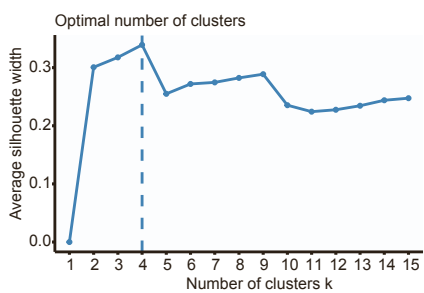
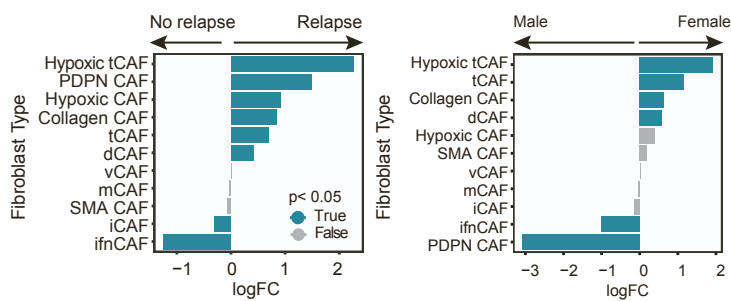
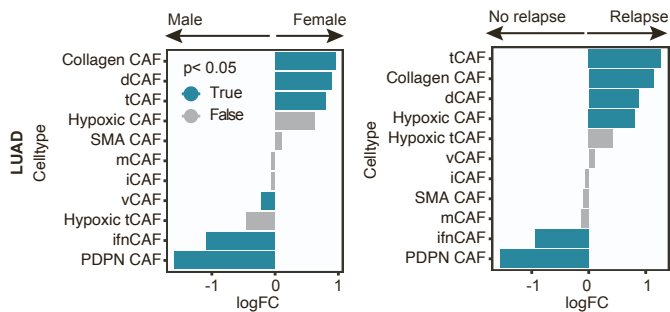
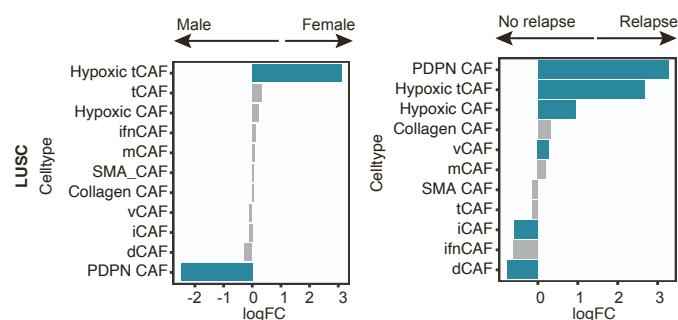
A**B****C****D****E****F**

Figure S3 – Correlation of CAF types with clinical data. Relates to figure 3.

- A) Differential abundance analysis for CAF types over tumour types (LUAD/LUSC)
- B) Boxplots comparing the proportions of CAF types between LUAD growth patterns (acinar, lepidic, micropapillary, papillary, solid); Kruskal-Wallis: * $p < 0.05$, ** $p < 0.01$, *** $p < 0.001$)
- C) Average silhouette width plot showing the optimal calculated cluster number for hierarchical clustering of CAF type proportions calculated per patient.
- D) Differential abundance analysis for CAF types over relapse and sex in both tumour types taken together.
- E) Differential abundance analysis for CAF type in LUAD for relapse and sex.
- F) Differential abundance analysis for CAF type in LUSC for relapse and sex

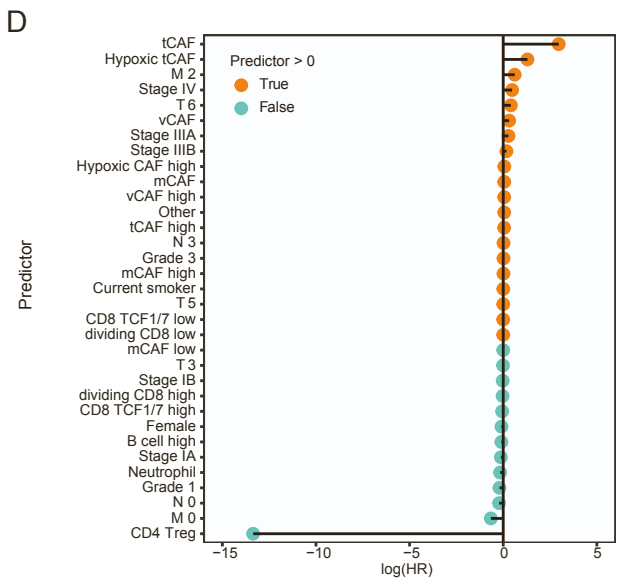
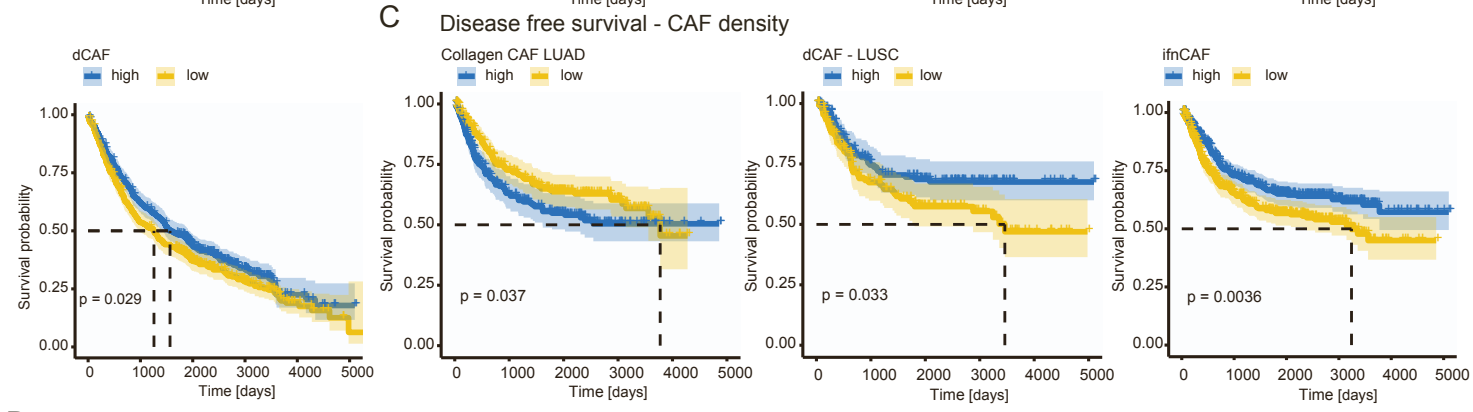
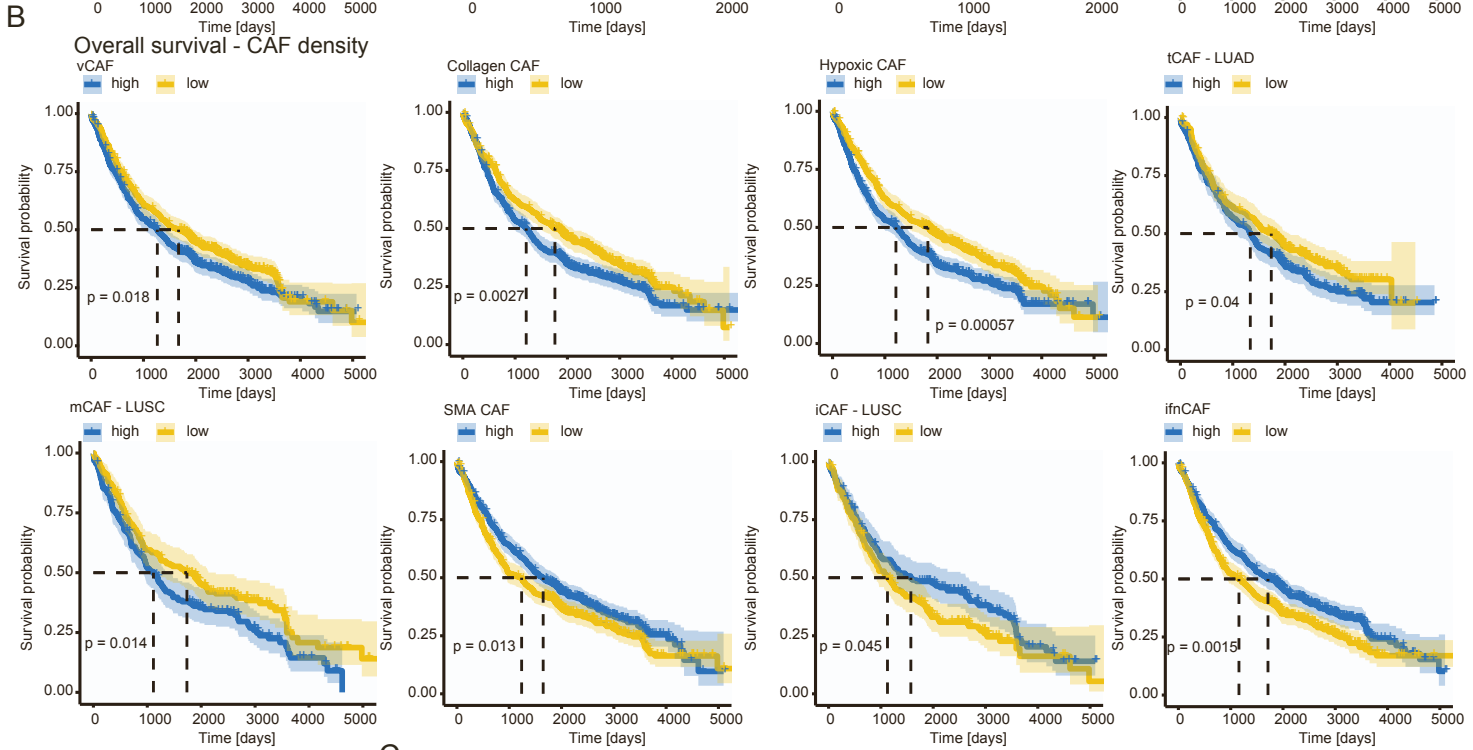
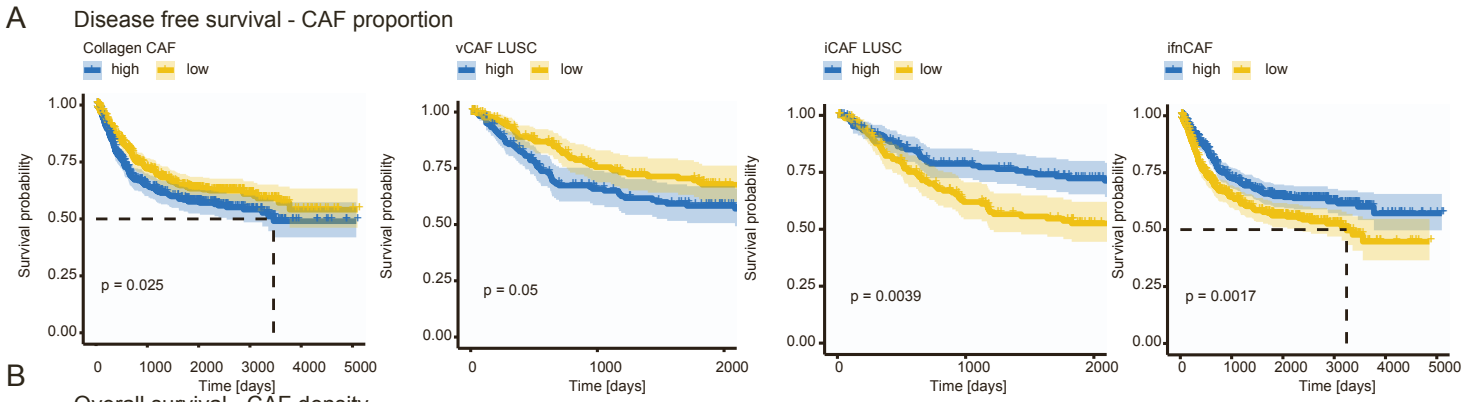


Figure S4 – Correlation of CAF types with survival data. Relates to figure 4.

- A) Kaplan-Meier plots of disease-free survival for patients stratified by median proportion into high and low for Collagen CAFs (all patients), vCAFs (LUSC), iCAFs (LUSC), and ifnCAFs (all patients).
- B) Kaplan-Meier plots of overall survival for patients stratified by median density into high and low for vCAFs (all patients), Collagen CAFs (all patients), hypoxic CAFs (all patients), tCAFs (LUAD), mCAFs (LUSC), SMA CAFs (all patients), iCAFs (LUSC), ifnCAFs (all patients), and dCAFs (all patients).
- C) Kaplan-Meier plots of disease-free survival for patients stratified by median density into high and low for Collagen CAFs (all patients), dCAFs (LUSC), and ifnCAFs (all patients).
- D) Lasso-regressed CoxPH model including mean CAF type density calculated per tumour core per patient as well as patient stratification into high and low for each CAF type (by median proportion) together with all available clinical data.

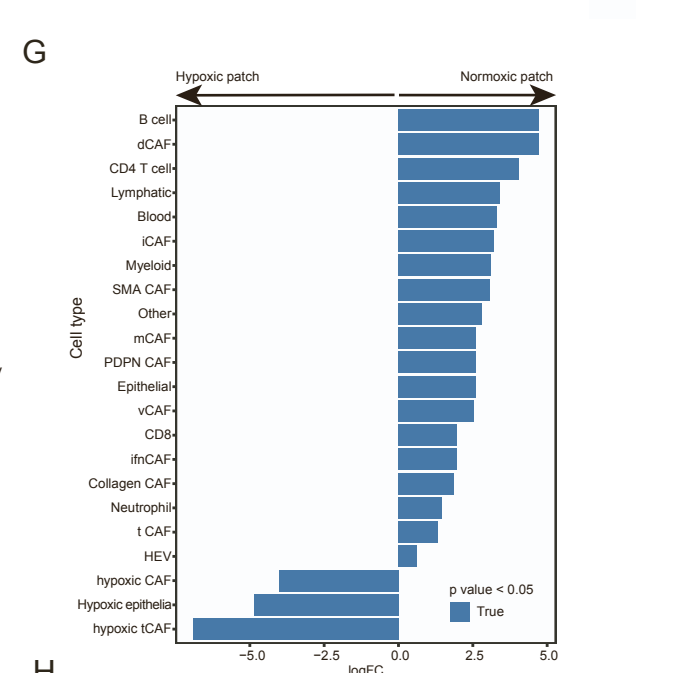
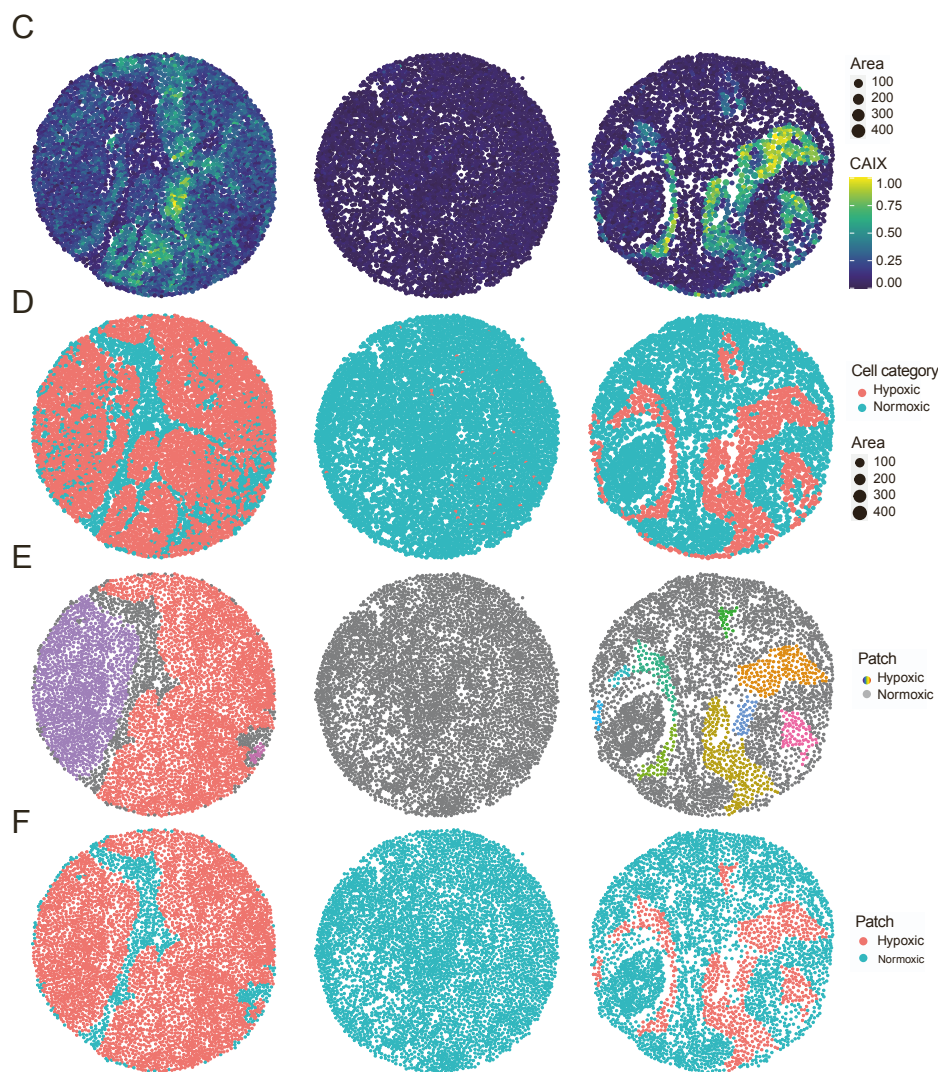
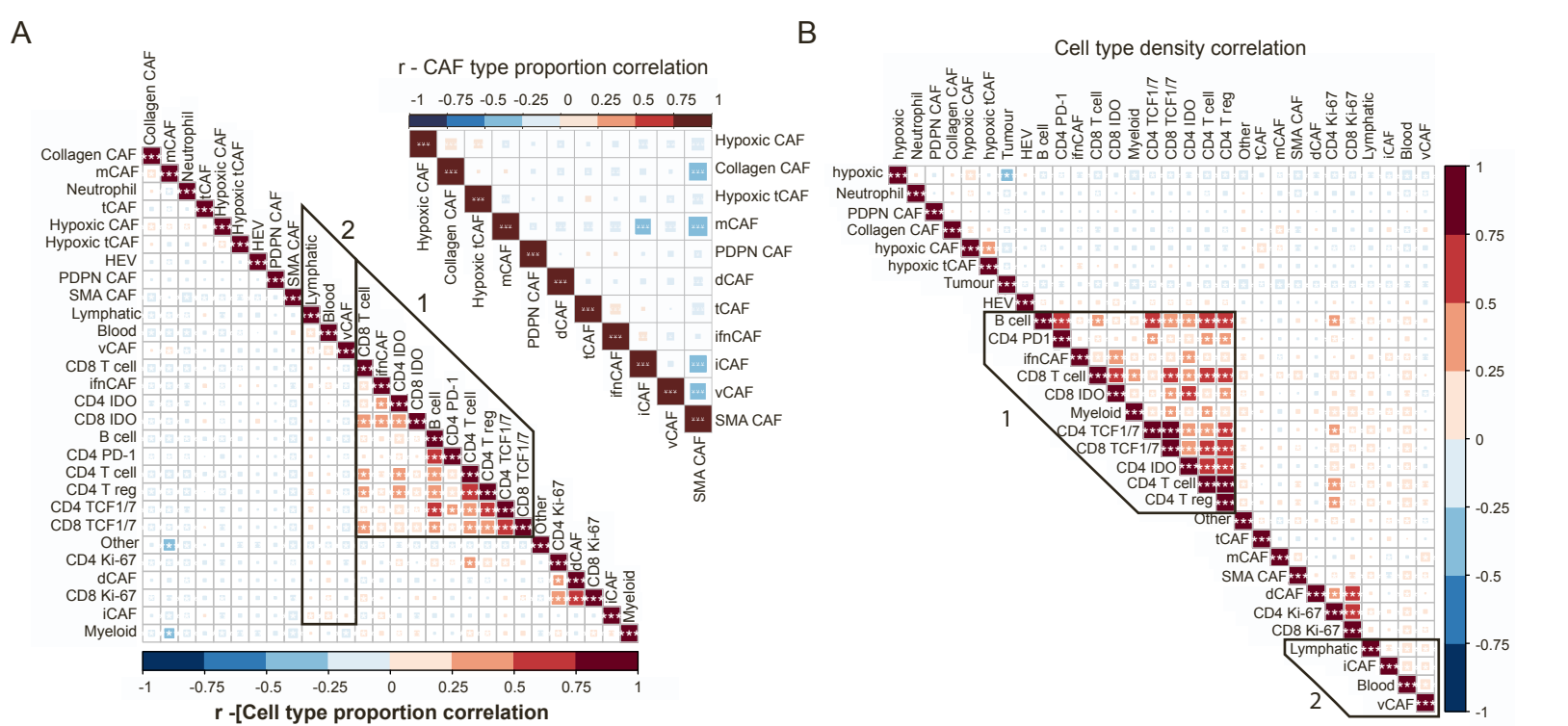
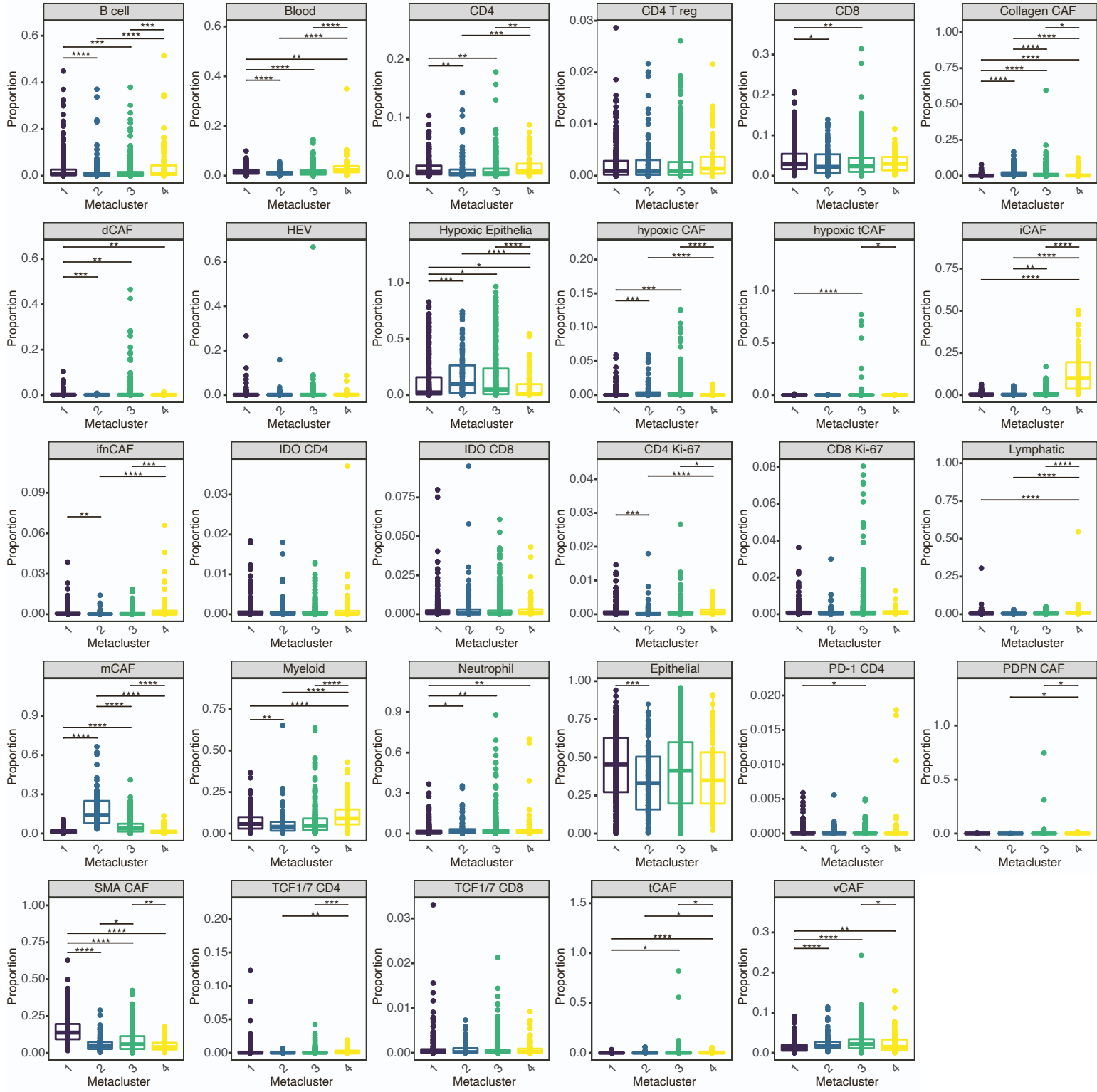


Figure S5 – Correlation of CAF types with other cells and hypoxia. Relates to figure 6.

- A) Correlations of the mean proportions per patient of all cell types (bottom left). Cluster 1 shows the correlation of ifnCAFs with various immune cells; cluster 2 shows the correlation of iCAFs with lymphatic and blood vessel cells and vCAFs. The second correlation matrix (top right) displays the correlation only of CAF types. (* $p < 0.05$, ** $p < 0.01$, *** $p < 0.001$).
- B) Correlations of the mean density per patient of all cell types (* $p < 0.05$, ** $p < 0.01$, *** $p < 0.001$). Cluster 1 shows the correlation of ifnCAFs with various immune cells; cluster 2 shows the correlation of iCAFs with lymphatic and blood vessel cells and vCAFs.
- C) Dot plot of three TMA cores showing the mean cellular expression of CAIX for each cell.
- D) Dot plot of three TMA cores (as in E) coloured by their categorisation as hypoxic (hypoxic epithelia, hypoxic tCAFs and hypoxic CAFs) and all normoxic cells.
- E) Dot plot of three TMA cores (as in E) showing patches calculated based on hypoxic cells.
- F) Dot plot of three TMA cores (as in E) showing patches defined as either hypoxic (red) or normoxic patches (blue).
- G) Differential abundance analysis comparing hypoxic versus normoxic patches.
- H) Correlations of all cells with hypoxic and normoxic patches.

A



**Supplementary Figure 6 – TME composition of patients stratified by CAF types.
Relates to figure 6.**

- A) Boxplots showing cellular enrichment of all cell types between the four meta-clustered patient groups (1, 2, 3, 4; Kruskal-Wallis: * $p < 0.05$, ** $p < 0.01$, *** $p < 0.001$).

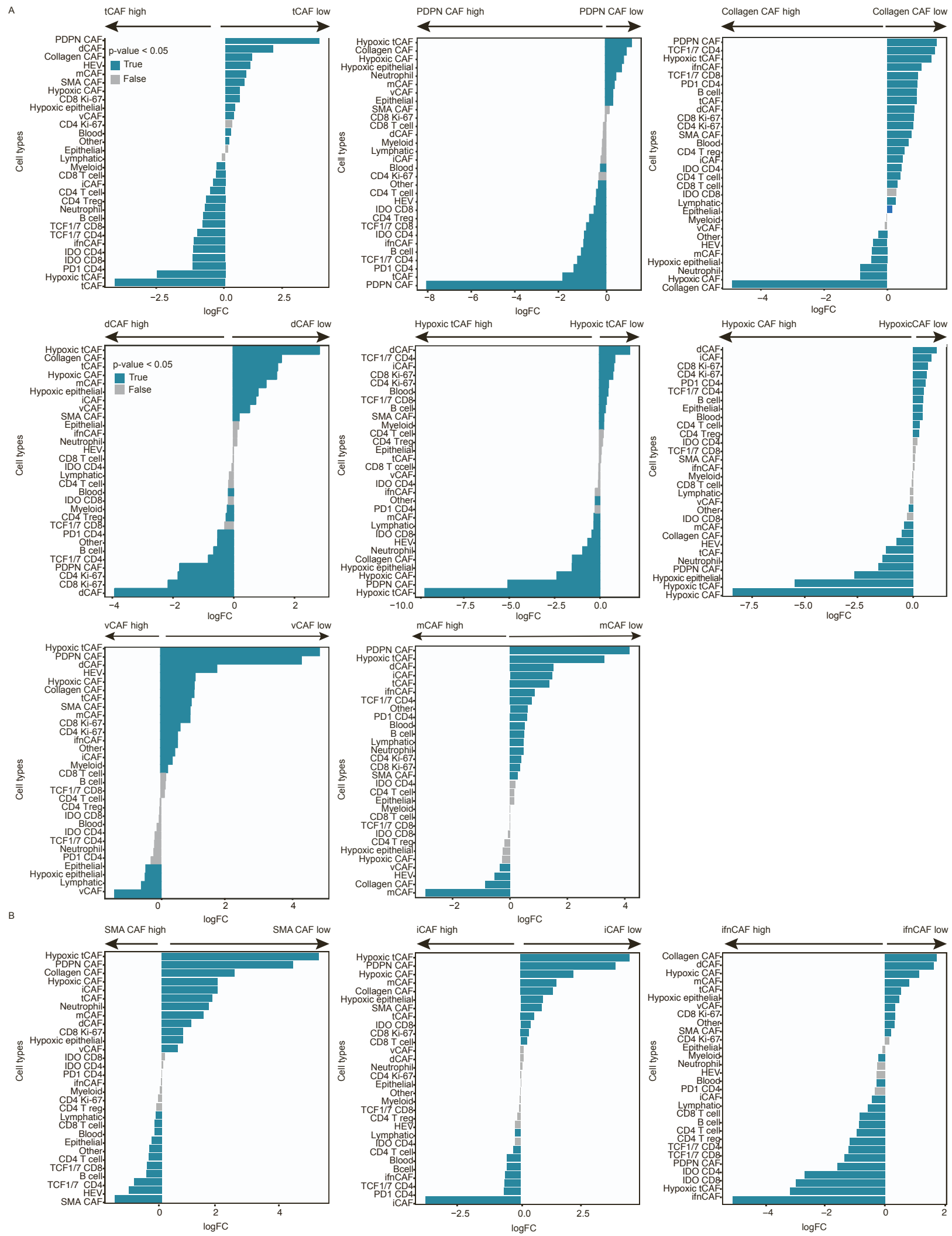


Figure S7 – TME composition of patients stratified by CAF types.
Relates to figure 6.

- A) Differential abundance analysis of all cell types between patients stratified as high or low based on mean proportions of poor-prognosis CAF types (tCAFs, PDPN CAFs, Collagen CAFs, dCAFs, hypoxic tCAFs, hypoxic CAFs, vCAFs and mCAFs).
- B) Differential abundance analysis of all cell types between patients stratified as high or low based on mean proportions of good-prognosis CAF types (SMA CAFs, iCAFs and ifnCAFs).

Supplementary tables and legends

Table S1 – Antibody panel. Related to STAR Methods

Metal Tag	Target	Antibody Clone	Lot	Provider	Catalogue Number	RRID
Y89	Myelo-peroxidase	Polyclonal	200304 5	Dako	A0398	AB_233 5676
In113	FSP1 / S100A4	Polyclonal	312695 3	Millipore	136784	AB_108 07552
In115	SMA	1A4	218390 0	eBioscience	14-9760-82	AB_257 2996
Pr141	Histone H3	D1H2	15	Cell Signaling Technology	4499BF	AB_105 44537
Nd142	CD11b	SP330	GR325 8740-1	Abcam	ab241408	AB_288 9379
Nd143	HLA-DR	TAL 1B5	GR322 2279-4	Abcam	ab20181	AB_445 401
Nd144	CD146	Polyclonal	ECL03 19041	R&D Systems	AF932	AB_355 721
Nd145	Cadherin-11	283416	VLT021 9091	R&D Systems	MAB1790	AB_207 6970
Nd146	FAP	Polyclonal	ZKW03 15081	R&D Systems	AF3715	AB_210 2369
Sm147	CD11b	M1/70	B18648 4	Biolegend	101202	AB_312 785
Nd148	VCAM1	EPR5047	GR325 5420-4	Abcam	ab215380	AB_289 4839
Sm149	CD20	L26	205997 6	eBioscience	14-0202-82	AB_107 34340
Nd150	CD68	KP1	213029 1	eBioscience	14-0688-82	AB_111 51139
Eu151	Indoleamine 2-3-dioxygenase	SP260	GR325 9345-2	Abcam	ab245737	AB_289 4840
Sm152	CD3	Polyclonal	GR322 9164-6	Dako	A0452	AB_233 5677

Eu153	Podoplanin	NC-08	B26083 4	Biolegend	337002	AB_159 5511
Sm154	CD11c	D3V1E	2	Cell Signaling Technology	45581BF	AB_279 9286
Gd155	Carbonic Anhydrase IX	Polyclonal	VNQ03 19011	R&D Systems	AF2188	AB_416 562
Gd156	CD73	D7F9A	2	Cell Signaling Technology	13160BF	AB_271 6625
Gd158	MMP9	D6O3H	4	Cell Signaling Technology	13667BF	AB_279 8289
Tb159	p75 / CD271	Polyclonal	ANT00 7AN07 02	Alomone labs	ANT-007	AB_203 9968
Dy161	CD10	E5P7S	2	Cell Signaling Technology	65534	AB_289 4842
Dy162	Vimentin	EPR3776	GR286 525-2	Abcam	ab193555	AB_281 4713
Dy163	FOXP3	236A/E7	212967 6	eBioscience	14-4777-82	AB_467 556
Dy164	CXCL13	Polyclonal	BAS03 17101	R&D Systems	AF801	AB_355 613
Ho165	PNAd	MECA-79	B25713 9	Biolegend	120802	AB_493 555
Er166	CD8a	C8/144B	213259 5	eBioscience	14-0085-82	AB_111 50240
Er167	Fibronectin	10/Fibro- nectin	625188 8	BD Biosciences	610078	AB_397 486
Er167	Collagen I	Polyclonal	GR325 3239-3	Abcam	ab34710	AB_731 684
Er168	LYVE-1	Polyclonal	KPY01 19052	R&D Systems	AF2089	AB_355 144
Tm169	CD140b	Y92	GR296 584-4	Abcam	ab215978	AB_289 4841
Er170	CD34	EP373Y	GR327 1518-1	Abcam	ab198395	AB_288 9381

Yb171	CD4	Polyclonal	YS071 8031	R&D Systems	AF-379-NA	AB_354 469
Yb172	vWF	poly wwf	332299 8	Millipore	AB7356	AB_922 16
Yb172	CD31	EPR3094	GR322 9164-6	Abcam	ab207090	AB_288 9382
Yb173	CXCL12 / SDF-1	79018	JOJ051 9031	R&D Systems	MAB350-100	AB_208 8149
Yb174	CCL21 / 6Ckine	Polyclonal	AYJ218 071	R&D Systems	AF366	AB_355 327
Lu175	Keratin Epithelial	AE3	325545 7	Millipore	MAB1611	AB_213 4409
Lu175	Pan Cytokeratin	AE1	325291 0	Millipore	MAB1612	AB_213 2794
Pt194	Ki-67	B56	811675 1	Becton Dickinson	556003	AB_396 287
Bi209	CD45	2B11	200342 2	eBioscience	14-9457-82	AB_110 63696

Table S1. List of all antibodies used in this study, their respective metal tag, clone number and vendor information, RRID (Research Resource Identifiers) and catalogue number.

Table S2 – Distribution of different cell classes in the stromal and tumour compartment. Related to STAR Methods

	Stroma [n]	Stroma [%]	Tumour [n]	Tumour [%]
Fibroblast	894478	82.3	192200	17.7
Immune	522302	63.5	299903	36.5
Other	387435	65.8	201453	34.2
T cell	265970	74.5	90939	25.5
Tumour	149901	5.0	2829811	95.0
vessel	124863	83.2	25199	16.8

Table S2. Number of cells and percentage within tumour and stroma subsets.

Table S3 – Number of cells in bins measured from the tumour-stroma border. Related to STAR Methods

Bins in μm from tumour-stroma border	Area	Fibroblast [n]	Immune [n]	Other [n]	T cell [n]	Tumour [n]	Vessel [n]
(>0)	Tumour	192100	299765	201349	90902	2829644	25183
-10 to -0	Stroma – tumour interface	299316	179225	127500	76138	126899	45952
-30 to -0	Stroma	598811	359337	257938	164075	144455	89846
-60 to 30	Stroma	155405	90191	71943	52227	3691	19364
-90 to -60	Stroma	63052	34494	27229	22389	995	6887
-120 to -90	Stroma	31572	17255	12560	11408	449	3416
-150 to -120	Stroma	17349	8971	6387	6202	217	1951
(-150)	Stroma	28389	12192	11482	9706	261	3415

Table S3. Number of cells in different bins from the tumour stroma border.